Acta Materialia Transylvanica 7/1. (2024) 08–13.
DOI: Hungarian: https://doi.org/10.33923/amt-2024-01-02
English: https://doi.org/10.33924/amt-2024-01-02

Examination of the Forming Properties of Vehicle Body Panels

Richárd BORBÉLY,[1] Martin László KÖLÜS,[1] Gábor József BÉRES[1]

John von Neumann University, GAMF Faculty of Engineering and Computer Science, Department of Innovative Vehicles and Materials, Kecskemét, Hungary, borbely.richard@nje.hu

Abstract

During vehicle design, the mass of the components and their resistance to collision are important criteria, as they affect fuel consumption and make the vehicle safer. In this study, we examined the deformation of high-strength materials commonly used in the automotive industry in the form of tailored welded blanks. Tests were conducted both in an experimental environment and in a simulation environment, measuring the punch displacement associated with the specimens to characterize the deformation. In designing the specimens, the weld seam was placed perpendicular and parallel to the rolling direction, thus creating different deformation states.

Keywords: *forming limit diagram, sheet metal forming, tailor welded blanks.*

1. Introduction

When designing vehicles, weight plays an important role as a criterion. By reducing weight, the fuel consumption of vehicles can be improved. Lowering fuel consumption not only makes vehicle operation more economical, but it also helps to meet increasingly stringent emission standards. It is important to note that in addition to emission requirements, numerous other equally important requirements must be considered during vehicle design, such as the collision resistance of the vehicle body, which is primarily ensured by the strength of the material. In the industry, three different methods are generally used to reduce weight. The first method is the use of high-strength, lightweight materials, known as HSS (High Strength Steel), a group of which includes dual-phase steels. These materials are characterized by excellent strength properties due to their special microstructure, allowing the required strength to be ensured with thinner sheets in specific applications. Another increasingly prevalent method today is the application of optimization techniques in structural design, such as optimizing material use or geometry based on load distribution.

The third option involves manufacturing techniques such as the use of tailor welded blanks and various hot forming processes. Among these methods, tailor welded blanks offer significant potential for improving vehicle safety and reducing weight, which can also lower manufacturing costs through reduced tooling expenses or shorter production times. The individual parts of tailor welded blanks are tailored in size, thickness, and material quality depending on the purpose of the installation location [1, 2]. Furthermore, their application can improve the dimensional accuracy of components by potentially replacing joining processes during assembly. In this study, we analyzed the interaction of different properties of blank sections with respect to formability using the finite element method with the help of AutoFormR7 simulation software [3, 4].

2. Materials

For the selection of materials needed for the production of tailor welded blanks, we chose traditional and high-strength steels that are commonly used in the automotive industry.

2.1. Low-carbon steels

Among traditional low-carbon steels, the HC340LA cold-rolled base material was selected. The low carbon content allows for easy machinability, formability, and weldability. Thanks to cold rolling, it also features good surface quality, shape, and dimensional accuracy. This type of material is mainly suitable for applications where machinability is more significant than the load-bearing capacity or strength of the finished part.

2.2. High-strength steels

Dual-phase steels are second-generation high-strength steels primarily used in the automotive industry. In these steels, the combination of soft ferrite and hard martensite components provides high strength and good formability. The characteristics of the material depend on the ferrite/martensite ratio and the distribution of martensite islands. Dual-phase steels exhibit outstanding tensile strength but do not have a distinct yield point. Martensite generally constitutes 5–30% of the microstructure, but in exceptionally high tensile strength materials, it can reach up to 40%. These materials allow for reducing damage during vehicle collisions without significantly increasing the vehicle's weight. In the test samples, HCT600X and HCT980X materials were welded separately to HC340LA material in each case.

3. Tailor-welded blanks

To conduct the tests, samples were produced in advance, which are necessary for the measurements carried out in real conditions. Tailor welded blanks consist of various properties and sizes of sheets that are joined using some welding method. These blanks present challenges in plastic forming, partly due to the presence of the weld seam. Several studies have already examined the weld seam and its surroundings to map the effects of different forming processes [5, 6].

In our case, the sheet blanks were joined using laser welding. The welding was performed without filler material, and to protect the weld seam, we used 4.6 purity argon shielding gas at a flow rate of 18 liters per minute, but only provided gas protection on the crown side. The gas was supplied by an external nozzle. In laser welding, the shape and power of the laser beam are influenced by numerous parameters, which are detailed in the MSZ EN ISO 11145 standard [7]. We selected the welding parameters based on our previous experiences, as presented in Table 1 [8]. The aim of the article is not to discuss the quality of the welding; rather, welding served the sole function of creating a solid bond between the two sheet materials. Furthermore, during the numerical analysis, the welding parameters were not utilized, as the software interprets the bonding technology differently from reality.

Table 1. *Welding parameters for HC340LA-HCT600X and HC340LA-HCT980X material combinations*

Pairs	HC340LA-HCT600X	HC340LA-HCT980X
Welding speed, V_h (m/min)	2.5	2.5
Continuous power output, P (kW)	1.2	1.2
Focus position (mm)	0	0
Focus spot area, A (mm^2)	0.0394	0.0394
Heat input, Q (J)	1200	1200
Power density, Q/A (W/cm^2)	$3.05 \cdot 10^6$	$3.05 \cdot 10^6$
Specific heat input, Q/v_{heg} (J/cm^2)	288	288

4. Numerical analysis

The simulation studies were conducted using the AutoFormR7 finite element software, which is one of the most advanced software tools in the field of sheet metal forming.

4.1. Tool layout

During the setup of the simulation environment, the input data was entered into the software based on realistic values. Accordingly, for determining the size and position of the tool geometries, we used a Nakazima test tool setup that can be mounted on an Erichsen 142-40 type universal sheet metal testing machine. The arrangement of forming tools and the layout of sample parts are depicted in Figures 1 and 2 within the simulation environment

In the depiction, the restraining ring is not shown, as it appears not as a geometry but as a constraint in the software. The diameter of the pull ring is 160 mm, and its iron cross-section is 15 mm. The position of the pull ring can be seen in Figure 3.

4.2. Input parameters

For achieving the most accurate simulation results, we provided the mechanical properties of the materials under investigation to correspond with reality. Therefore, from the premanufactured sample material, sheet specimens were fabricated for tensile testing, and the results of these tests were converted into input parameters.

We described the flow curves of the materials using the combined Swift-Hockett-Sherby equa-

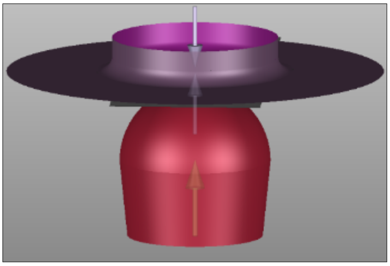

Fig. 1. *Tool layout in AutoFormR7 software (side view).*

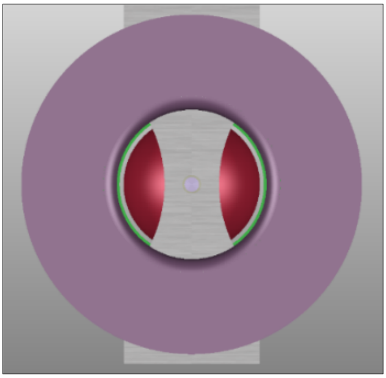

Fig. 2. *Sool layout in AutoFormR7 software (top view).*

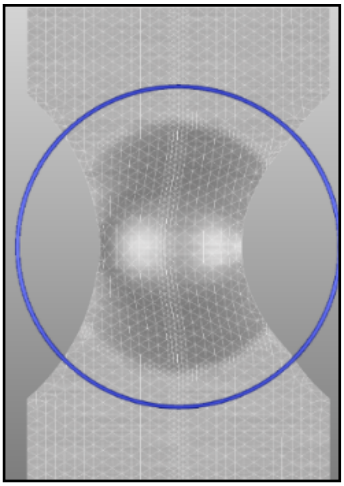

Fig. 3. *The position of the pull ring (blue line).*

tion **[9]** the input values of which are summarized in **Table 2.**

The parameters listed in the table are as follows: s sheet thickness, m hardening parameter, C hardening constants, σ_i true stress, σ_{sat} saturation stress, a and p weighting parameter, σ_0 initial yield stress, R_m ultimate tensile strength.

Table. 2. *Flow curve input data*

		Material	HC 340LA	HCT 600X	HCT 980X
		s (mm)	1	1	1
Flow curve parameters	Swift	ε_0	0.02	0.04	0.01
		m	0.22	0.16	0.098
		C (MPa)	578	1044	1578
	Hockett–Sherby	σ_i (MPa)	229	448	788
		σ_{sat} (MPa)	456	780	1160
		a	8.6	21	102
		p	0.81	0.812	0.785
		σ_0 (MPa)	235	443	798.4
		R_m (MPa)	343	668.9	1122

In order to appropriately model sheet metal forming processes, it is also necessary to determine the flow stress condition. The equation describing this was also determined from tensile tests by fabricating specimens perpendicular to the rolling direction, parallel to it, and at a 45-degree angle to it. For determining the forming limit diagram, material parameters according to the Arcelor V9 model **[10, 11]** developed by F. Cayssials were used. The purpose of the study is not to compile and edit the forming limit diagrams of various materials. The aim of the study is to examine under identical conditions how different material pairings affect each other. The mentioned data is summarized in **Table. 3**.

Table 3. *Input data for forming limit diagram*

	Material	HC340LA	HCT600X	HCT980X
Barlat' 89 model [9]	r_0	1.82	0.865	0.73
	r_{45}	1.31	0.929	0.894
	r_{90}	2.38	0.941	0.828
	M	6	6	6
	r_m	1.71	0.916	0.837
Arcelor V9 model	$A_{G,90}$ (%)	20.5	12.5	6.3
	$R_{m,90}$ (MPa)	325	669	1111

The parameters listed in the table are as follows: r_0 plastic strain ratio at 0°, r_{45} plastic strain ratio at 45°, r_{90} plastic strain ratio at 90°, M weighting parameter, r_m average plastic strain ratio, $A_{G,90}$, $R_{m,90}$.

4.3. The test specimens examined in the simulation

When selecting the geometry of the test specimens, in line with the tool geometries, various square specimens with different bridge widths (20-200 mm) were used, as commonly employed in Nakazima testing. The selection of test specimen geometries aimed to comprehensively cover the possible major strain regions of the forming limit diagram (FLD). Due to the different stress states created by the varied test specimen designs, the location of fracture is not constant; failure will be observed to some extent at varying locations. The utilized test specimen geometries are illustrated in Figure 4.

As mentioned earlier, the formation of different material pairings was done through laser welding. However, both in reality and in the simulation software, the orientation of the welding seam differed. Based on the orientation of the welding seam, two cases were distinguished: Case ‚A' where the welding seam (red line) is perpendicular to the rolling direction (colored line), and Case ‚B' where the welding seam is parallel to the rolling direction. Figures 5. and 6 illustrate these two types on a randomly selected test specimen.

5. Simulation results

During the evaluation of the results, the basis of comparison was provided by the stamping displacement values achieved until the failure of the

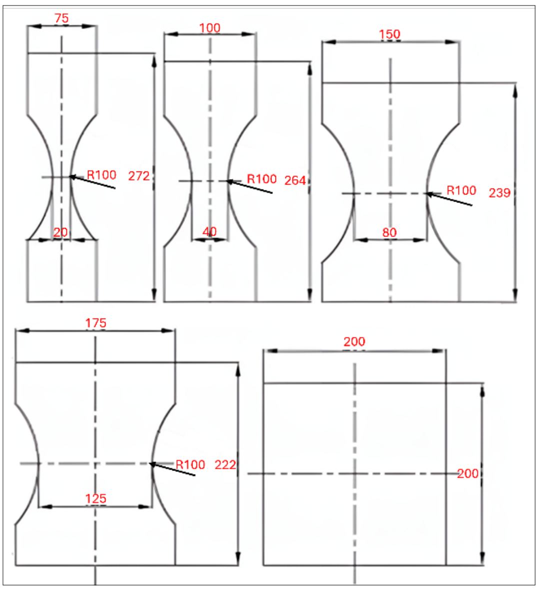

Fig. 4. *Test specimen geometries*

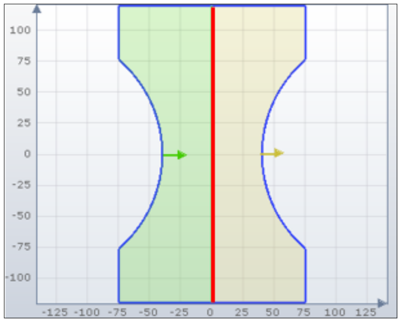

Fig. 5. *Location of weld seam type „A*

Fig. 6. *Location of weld seam, type „B"*

specimens with different material pairings and welding seam orientations. The values listed in Tables 5–8 thus illustrate the stamping displacement until failure of the specimens.

5.1. „A" type specimens

In the case of specimens with type ‚A' weld seams, perpendicular to the rolling direction, the evaluation of results involved continuing the forming process until one of the constituent materials reached its forming limit diagram. For the HC340LA-HCT600X material pairing, the results are summarized in Table 4, while for the HC340LA-HCT980X TWB, they are presented in Table 5. In the tables, the bridge width refers to the smallest width of the specimens.

Table 4. *Material pairing of HC340LA-HCT600X with type „A" weld seam*

„A" type, HC340LA-HCT600X		
Bridge width (mm)	**Punch stroke HC340LA (mm)**	**Punch stroke HCT600X (mm)**
20	35.2	28.7
40	38.2	32.2
80	41.5	35.2
125	44.2	36.7
200	47.7	43.2

5. táblázat. *Material pairing of HC340LA-HCT980X with type „A" weld seam*

„A" type, HC340LA-HCT980X		
Bridge width (mm)	**Punch stroke HC340LA (mm)**	**Punch stroke HCT980X (mm)**
20	31.7	22.7
40	35.7	26.2
80	44.1	29.2
125	41.3	30.7
200	41.2	30.2

In this seam arrangement, except for the specimen with a bridge width of 200, the material with higher strength and simultaneously lower formability reached its forming limit diagram first. Therefore, the global formability was solely determined by the formability of the material with higher strength.

5.2. „B" type specimens

In the case of specimens with type „B" weld seams, parallel to the rolling direction, the evaluation of results involved continuing the forming process until one of the materials reached its forming limit diagram. The results are summarized in **Tables 6** and 7.

Table 6. *Material pairing of HC340LA-HCT600X with type „B" weld seam*

„B" típus HC340LA-HCT600X		
Bridge width (mm)	**Punch stroke HC340LA (mm)**	**Punch stroke HCT600X (mm)**
20	31.2	–
40	34.7	–
80	31.7	–
125	30.2	–
200	34.7	38.2

Table 7. *Material pairing of HC340LA-HCT980X with type „B" weld seam*

„B" type, HC340LA-HCT980X		
Bridge width (mm)	**Punch stroke HC340LA (mm)**	**Punch stroke HCT980X (mm)**
20	31.2	–
40	33.7	–
80	31.2	–
125	32.7	–
200	30.2	32.2

In terms of results, it's also important for us to know what stamping displacement a HC-340LA-HC340LA pairing yields under identical conditions in case „B". The results of this will be illustrated in **Table 8**.

Table 8. *Material pairing of HC340LA-HC340LA with type „B" weld seam*

„B" type, HC340LA-HC340LA		
Bridge width (mm)	**Punch stroke HC340LA (mm)**	**Punch stroke HC340LA (mm)**
20	36.7	36.7
40	39.6	39.6
80	44.8	44.8
125	45.8	45.8
200	54.1	54.1

From this, it can be observed that the hindering effect of deformation by the higher-strength layer significantly manifests itself on the lower-strength side, which always corresponds to the failure side in the „B" cases. Global deformation deteriorates more significantly in specimens with larger bridge widths. This can be explained by the fact that the three-axis deformation state in these specimens is reduced to a planar deformation state.

6. Conclusions

In our paper, we examined the global formability of customized welded sheets and the interaction between individual layers. The physical testing of the specimens is currently ongoing, and we primarily presented simulation results. We investigated two cases based on the orientation of the welding seam, with two different TWB configurations composed of different components, in five different deformation states each. Based on the results obtained, we can make two observations:

- In case ‚A', the plates composing the specimens deformed collectively; therefore, the material with the forming limit diagram positioned lower (higher strength) experienced failure earlier, with the exception of the 200x200 mm case;
- In case ‚B', the lower strength material (HC-340LA) consistently fails earlier. Furthermore, it can be noted that the failure point is significantly unaffected by the different strength materials (HCT600X-HCT980X) within this strength range.

As part of the research, our further aim is to investigate material pairings where the HC340LA material is paired with other materials of varying strength levels, in order to observe the effect of strength differences on global formability. Additionally, we will conduct tests on existing specimens in real-world conditions, following the method outlined in the simulation environment, and compare their results with the simulation findings.

References

[1] Kinsey B., Wu X. (szerk.): *Tailor welded blanks for advanced manufacturing.* Elsevier, Cambridge, 2011. 95–115.

[2] Safdarian R.: *Forming limit diagram prediction of tailor welded blank by modified M-K model.* Mech. Res. Commun., 67. (2015) 47–57. https://doi.org/10.1016/j.mechrescom.2015.05.004

[3] Korouyeh R. S., Naeini H. M., Liaghat G. H., Kasaei M. M.: *Investigation of weld line movement in tailor welded blank forming*. In: Advanced Materials Research, Trans Tech Publications Ltd., 2012. 39–44. https://doi.org/10.4028/scientific5/AMR.445.39

[4] Safdarian R.: *The effects of strength ratio on the forming limit diagram of tailor-welded blanks*. Ironmaking Steelmaking, 45/1. (2018) 17–24. https://doi.org/10.1080/03019233.2016.1235371

[5] Merklein M., Johannes M., Lechner M., Kuppert A.: *A review on tailored blanks – Production, applications and evaluation*. Journal of Material Processing Technology, 214/2. (2014) 151–164. https://doi.org/10.1016/j.jmatprotec.2013.08.015

[6] Ahmetoglu M. A., Brouwres D., Shulkin L., Taupin L., Kinzel G. L., Altan T.: *Deep drawing of round cups from tailor-welded blanks.* Journal of Material Processing Technology, 53/3-4. (1995) 684–696. https://doi.org/10.1016/0924-0136(94)01767-U

[7] Béres G. J., Danyi J. Végvári F., Tisza M.: The present body in white materials. Gradus, 2/2. (2015) 209–224.

[8] Kovács Zs. F., Béres G., Weltsch Z.: *The Investigation of DC and DP steels weldability by laser beam*. Gradus, 4/2. (2017) 311–317 .

[9] Barlat F., Lian K.: *Plastic behavior and stretchability of sheet metals. Part I: A yield function for orthotropic sheets under plane stress conditions.* International Journal of Plasticity, 5/1. (1989) 51–66. https://doi.org/10.1016/0749-6419(89)90019-3

[10] Cayssials F.: *Sheet Metal Forming Beyond 2000.* Proc. of the 20th Biennial [IDDRG] Congress, Brussels, Belgium (Liege: CRM), 1998. 443−54.

[11] Cayssials F., Lemoine X.: *Proc. of the 24th IDDRG Congress*. Besancon, France, 2005. 1–8.